

sweet- An Open Source Modular Platform for Contactless Hand Vascular Biometric Experiments

David Geissbühler, Sushil Bhattacharjee, Ketan Kotwal,
Guillaume Clivaz, and Sébastien Marcel

Idiap Research Institute, Switzerland

Abstract—Current finger-vein or palm-vein recognition systems usually require direct contact of the subject with the apparatus. This can be problematic in environments where hygiene is of primary importance. In this work we present a contactless vascular biometrics sensor platform named *sweet* which can be used for hand vascular biometrics studies (wrist, palm, and finger-vein) and surface features such as palmprint. It supports several acquisition modalities such as multi-spectral Near-Infrared (NIR), RGB-color, Stereo Vision (SV) and Photometric Stereo (PS). Using this platform we collect a dataset consisting of the fingers, palm and wrist vascular data of 120 subjects and develop a powerful 3D pipeline for the pre-processing of this data. We then present biometric experimental results, focusing on Finger-Vein Recognition (FVR). Finally, we discuss fusion of multiple modalities, such palm-vein combined with palm-print biometrics. The acquisition software, parts of the hardware design, the new FV dataset, as well as source-code for our experiments are publicly available for research purposes.

Index Terms—Vascular biometrics, Finger-Vein Recognition, Multi-Spectral Imaging, Stereoscopy, Photometric Stereo, Score-Fusion.

I. INTRODUCTION

Vascular Biometrics [1], [2], or Vein Recognition (VR), offers several advantages [3] such as convenience, high recognition accuracy, and robustness to spoofing over extrinsic biometric modalities such as face, fingerprint, or iris. Most existing FVR devices require the subject’s finger to be in contact with the device. They rely on transmissive Near-Infrared (NIR) illumination [4], [5], where the finger is placed between the illuminator and the camera. The NIR light is scattered in the finger-tissue and absorbed by oxygenated hemoglobin in the blood vessels. This design has the advantage that the sensor captures only light that has traveled through the finger and is robust to interference due to external light [6].

Direct contact with a biometric device can be a concern however, from the point of view of hygiene, which can be critical in environments such as hospitals where transmission of pathogens via surfaces should be mitigated [7]. Some systems require the finger to be placed in an enclosure which users may find uncomfortable [8].

Reflection-based vascular biometric systems, on the other hand, can be made contactless [9] as by their geometry the illuminator is facing the same direction as the sensor [10]. This family of sensors takes advantage of the penetration depth, typically a few millimeters, of NIR light into the skin

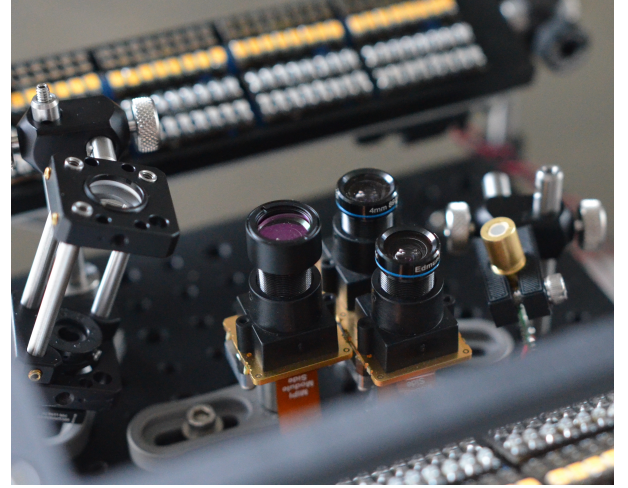


Fig. 1: Optical bench of the *sweet* sensor package.

tissue which enables capture of the shallow vein network. Unfortunately, this technique yields a signal of a much lower quality and is very sensitive to environmental conditions.

In this work we present a modular platform named *sweet* aimed at exploring several technologies and sensors with the goal of improving state-of-the-art contactless reflective vascular hand biometrics. Our device is able to acquire images of fingers, palm and wrist in several near-infrared (NIR) wavelengths, for vascular features, as well as in visible light (RGB), for surface features such as fingerprint and palmprint. Moreover, this platform also captures depth information using a pair of NIR cameras with laser pattern projectors and by varying the angle of incidence of the illumination source. This data can be combined to reconstruct the precise shape, texture and reflectivity map, throughout various wavelengths, of the target using Stereo Vision (SV), Photometric Stereo (PS) and 3D image-alignment, yielding high quality original data unavailable, to our knowledge, in commercial hand biometric sensors.

Besides introducing the hardware prototype, we also present FVR experiments to study the efficacy of our approach. The FVR experiments discussed here are based on a new dataset collected from 120 subjects using the *sweet* platform. While most currently available FVR sensors, including some of the most recent ones, require the user to present one finger at a time, our platform, by design, can capture vein-images of multiple fingers simultaneously by using large Field of View (FoV) optics and high resolution sensors. This, in turn, enables

us to combine information from several fingers, to increase the FVR accuracy and reduce the FV recognition HTER to 0.057%. These results demonstrate that the *sweet* platform offers state-of-the-art FVR performance.

This article is organized as follows. After a discussion about previous research related to the presented work in Section II, we describe the hardware design for *sweet* sensor platform in Section III. In Section IV we present the underlying software stack, pre-processing, calibration, SV depth inference and PS. FVR performance evaluated using a new dataset collected using the *sweet* platform are discussed in Section V. A brief summary and conclusions in Section VI close this paper.

II. RELATED WORK

Contactless vascular biometric systems [9] have been investigated for more than a decade. Reflective VR systems have been developed for finger [10], palm [11], [12], palm and finger [13], wrist [14] and forehead [15]. Yuan and Tang [16] have also proposed combining surface and vascular features such as palm-vein with palm-print.

Multi-spectral biometric systems [17] have been used for a variety of modalities and applications. Spinoulas *et al.* [18] use color RGB, NIR and Short-Wave Infrared (SWIR) illumination to improve face presentation attack detection (PAD). Multi-spectral data has been shown to improve iris recognition [19], and fingerprint recognition [20]. Hao *et al.* [21] have developed a multi-spectral imaging device for contactless palmprint recognition.

Using 3D depth information [22] for face PAD is now common in consumers products such as smartphones. Although Stereo Vision (SV) based VR methods have been recently proposed [23], these systems are still quite rare. Kauba *et al.* [24] propose a transmissive acquisition technique where the camera and illumination module rotates around the finger, whereas in [25] three cameras surround the finger. In [26] photometric stereo (PS) is proposed as biometric modality using 3D knuckle patterns on the fingers.

While most apparatus in biometric laboratories are expensive research prototype, the authors in [27] use a Raspberry Pi (RPI) platform for the acquisition computer and in [28] a RPi NoIR camera is employed as a sensor.

Newly proposed FVR algorithms are compared to the state-of-the-art using publicly available datasets such as SDUMLA-HMT [29], MMBNU_6000 [30], VERA-finger [4], UTFVP [31], and SCUT-SFVD [32]. One common characteristic of these datasets is that the biometric samples are single-finger ones. In contrast, FV samples in the presented dataset show four fingers together, which enables finger-fusion for robust FVR.

Early research in vascular biometrics relied on various hand-crafted features such as Repeated Line-Tracking (RLT) [33], maximum curvature (MC) [34], wide-line detection (WLD) [35]. These algorithms extract binary pixel-maps representing the vein-network in the biometric sample allowing to compare them. In this work we have used MC features.

Frequency-domain methods for FVR has also been proposed. Yang *et al.* [36] have used a bank of Gabor filters to

enhance veins at different scales and then construct a set of FVCodes that are compared using a Cosine-similarity function. This method is claimed to perform better than Miura's MC features [34]. These results, however, have been estimated over a proprietary, unpublished dataset. More recently, Kovač and Marák [37] have used Gabor filters to detect feature-points in vein-images. Speeded-up robust features (SURF) [38] are used to generate feature-descriptors for the selected feature-points, to construct biometric templates achieving an FVR accuracy of 99.94% on SDUMLA-HMT.

As a recent review [39] shows, several deep learning approaches for FVR have been proposed. Unlike for face-biometrics, publicly available FV datasets are not large enough to train a convolutional neural network (CNN) from scratch. Up to now, deep-learning based FVR approaches have adapted pre-trained CNNs through transfer-learning on FV datasets to construct feature-extractors. Besides actual FVR, deep-learning based methods have also been used for other purposes such as vein-segmentation, encryption, as well as vein-enhancement [40], [41] (see [39]). We note here the work of Bros *et al.* [40] proposing a Residual Convolutional Autoencoder (RCAE) for vein-enhancement that reduces the classification error on the UTVFP dataset from 2.1% to 1%. In the present work we have used this RCAE in our processing pipeline as well.

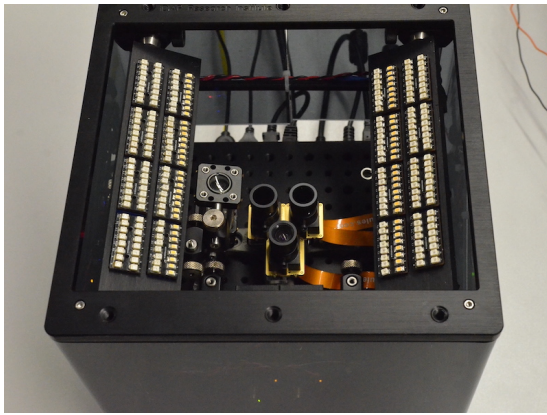
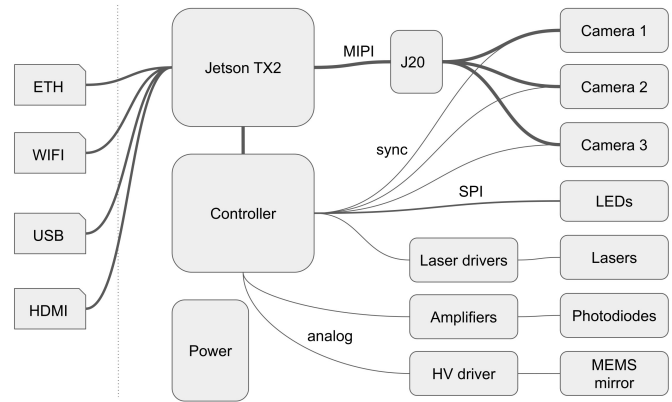
III. HARDWARE DESIGN

A. The *sweet* Sensor Platform

The main goal of this work is to test several sensors and technologies that can allow contactless VR and PAD with high accuracy. In order to mitigate the difficulties associated with contactless reflective acquisition, we follow a modular and extensible approach where several cameras, sensors, illumination devices and modalities are tested for performance. We chose to use focus our attention on sensors that are sufficiently affordable for consumer products, for instance by using small camera modules and cheap S-Mount lenses. Moreover, we hope that such new sensing technologies will be useful in other domains of Science such as medical research. For the present article, we focus our attention on the following acquisition modalities:

- NIR HD camera pair, with multi-spectral illumination at 850nm and 950nm, for vein recognition (VR).
- Color HD camera with white illumination, used for surface features and PAD.
- Stereo Vision (SV) depth measurement using the NIR camera pair and laser dot projectors.
- Photometric Stereo (PS) to obtain fine grained depth resolution and texture from a set of frames illuminated from different angles.

For this platform, we made the choice of using small camera sensors and miniaturized optics to have an image quality more comparable to consumer devices but also allowing us to have a small stereoscopic baseline adapted to short range depth sensing. This choice dictates the use of small embedded computer, integrated in the platform, that can interface with the low-level MIPI-CSI data link of these camera modules.

(a) *sweet* sensor top view.

(b) Connectivity diagram for the different sub systems.

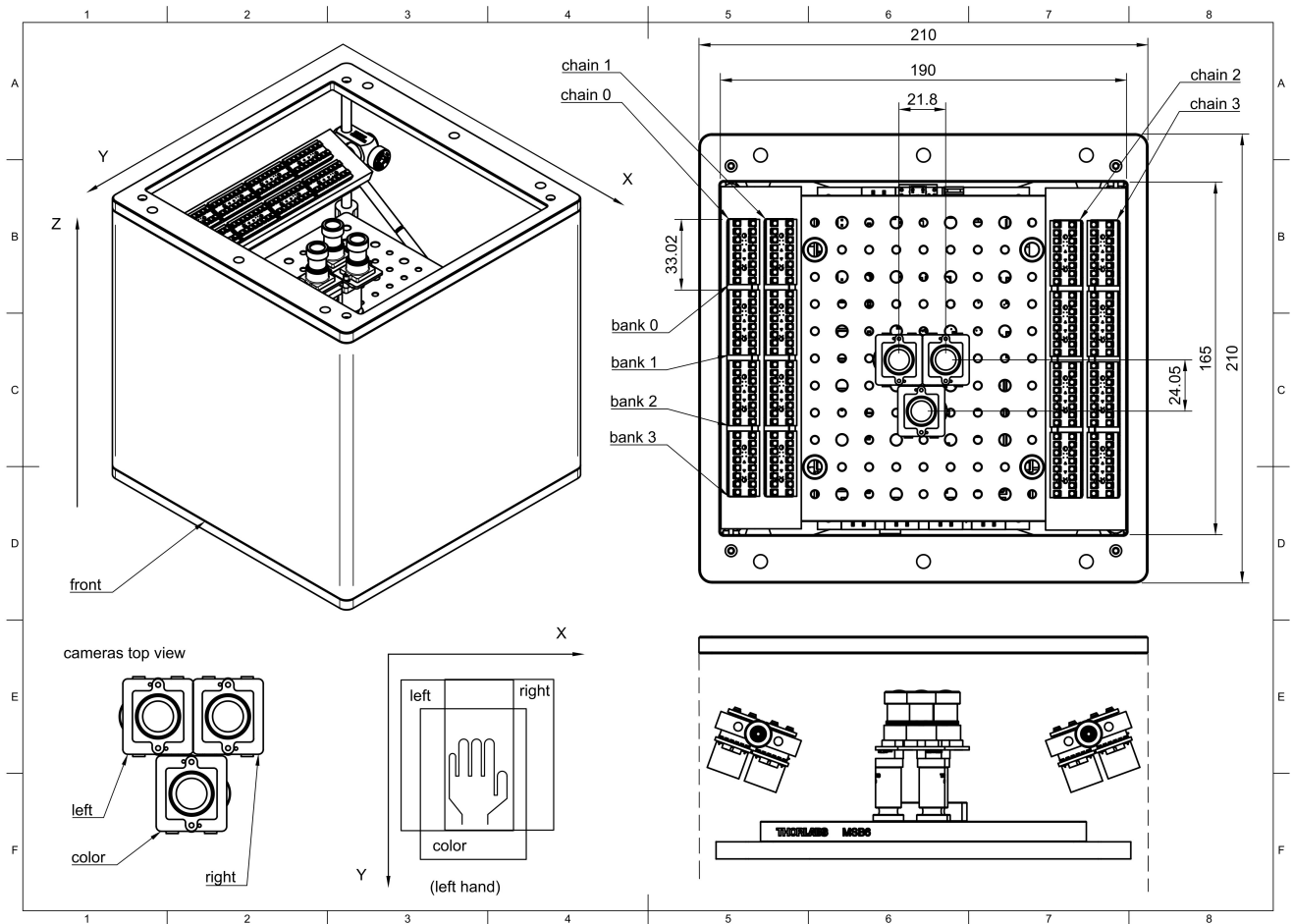
Fig. 2: The *sweet* sensor platform.

Fig. 3: From left to right, top to bottom: Coordinate system of the sensor, dimensional drawing of the sensor viewed from top, camera naming conventions and positioning, coordinate system of the captured images and cross section of the sensor showing illumination and camera positioning.

We selected a Jetson TX2 for this purpose, which also opens interesting possibilities for studying low power embedded algorithms.

A schematic diagram depicting the connection of the different subsystems of the device is shown in (Fig. 2b). The *sweet* sensor platform aims at integrating the various elements, cameras, illumination, computer and electronics in a small footprint, $21 \times 21 \times 21 \text{ cm}$, to allow simple operation for data capture. It is completed by a screen, a keyboard and a mouse and is used like a regular computer. Cameras and optical components are mounted on an optical breadboard to allow re-positioning and extension. The enclosure (Fig. 3) is made of two aluminum plates connected by four 6 mm stainless rods along which components can slide.

B. Camera and Optics

For this platform we selected a Sony IMX296 CMOS sensor board ¹ a sensor with good sensitivity in the NIR domain capable of capturing 950 nm light. This sensor has a global shutter allowing for accurate synchronization required by SV. It communicates with the host via a MIPI-CSI². It provides 1440×1080 pixels (1.58 M pixels) with 10 bits resolution, is capable of 60 Frames Per Second (FPS), and with a acceptable sensitivity in the NIR range provide it is complemented with 750 nm low-pass filters. It has 24 dB of analog gain and 24 dB of digital gain, the pixels are $3.4 \mu\text{m} \times 3.4 \mu\text{m}$ for a total active area of $4.9 \times 3.7 \text{ mm}$, i.e. a 6.3 mm diagonal or $1/2.9$ type sensor.

The sensor size constraints the focal length f of the lens as the FoV should be large enough to capture an hand at a relatively short distance and wider FoV leads to higher lens distortion. We choose to use a $f = 4 \text{ mm}$ lens ³ which give horizontal, vertical and diagonal angles of view of 49.64° , 62.97° and 75.01° respectively. At a working distance of 120 mm , the horizontal, vertical and diagonal FoV in a first order approximation is 111 mm , 147 mm and 184 mm respectively. Sensors are in portrait orientation.

The use of S-mount M12 lenses constrains the use of fixed aperture optics. On one hand a bigger aperture gives an advantage in term of collected light, on the other hand bigger apertures reduce then usable Depth of Field (DoF). This last quantity can be computed from the formulas

$$H = \frac{f^2}{Nc} + f \quad (1)$$

$$D_n = \frac{s(H-f)}{H+s-2f} \quad (2)$$

$$D_f = \frac{s(H-f)}{H-s} \quad (3)$$

where H is the hyper-focal distance, $f = 4 \text{ mm}$ is the focal length, $N = f/2.5$ the f-number of the lens, $c = 4 \mu\text{m}$ the circle of confusion, s the focussed distance and D_n and D_f

the near and far limits. With a focussed distance $s = 120 \text{ mm}$ we get $H = 1.6 \text{ m}$, $D_n = 112 \text{ mm}$, $D_f = 129 \text{ mm}$ and

$$\Delta = D_f - D_n = 17 \text{ mm}. \quad (4)$$

The DoF Δ of only 17 mm only correspond to an area where sharpness is maximal, the final usable range is bigger in practice. A smaller f-number of $f/5$ would lead to a double DoF ($\Delta = 35.5 \text{ mm}$) range at the expense of a four time lower collected light.

C. Jetson Acquisition and Processing Platform

The choice of MIPI CSI camera modules severely constrains the available platforms that can interface several of them. While Field Programmable Gate Array (FPGA) are ideal for these purposes, we instead chose to use an NVIDIA Jetson TX2 that can acquire up to six 2-lanes camera modules. In addition of being much simpler to setup than an FPGA, these System-on-Module (SoM) are based on a multi-core ARM architecture coupled with a relatively powerful GPUs allowing the use of ML frameworks such as PyTorch. For this work a Jetson TX2 Developer Kit, with and Auvidia J20 camera expansion card, providing a dual-core NVIDIA Denver 2 64-Bit CPU, 4 ARM Cortex-A57 MPCore low power cores, an NVIDIA Pascal GPU with 256 CUDA cores, 8GB of shared RAM and 32GB of eMMC flash memory that is extended with a 512GB external SSD.

D. Illumination, Lasers and Controller

For LED illumination we use a modular approach first developed in [18] using 4 banks of 4 interchangeable modules (Fig. 3), each with up to 16 surface mounted LEDs. Each of the 256 LED can be addressed individually in both current, up to 57 mA per device, and Pulse Width Modulation (PWM). These modules are based on the PCA9745B chip⁴ thus requiring no LEDs resistor, are daisy chained and controlled by a serial SPI signal. The LED are powered by a dedicated and robust 5 V DCDC Power Supply Unit (PSU) module delivering up to 8 A to the illumination system. Switching all 256 LEDs takes approximately 1 ms . For legal reasons, we cannot release this simple design.

Since commercial laser drivers are bulky and expensive, we developed our own custom laser drivers boards based on the IC-NZN⁵ chip. These are capable of driving diode lasers in both optical output power (APC) or constant current (ACC) modes, switching up to 155 MHz with an external signal, interface with most laser diodes types (P,N,M) and provide a convenient PMOD⁶ interface. This design is released under an open source license alongside this paper.

In order to control camera triggering in real-time, LEDs dimming and lasers switching, an additional custom embedded controller board is used. This board is based on a Teensy 4.1 module⁷ and will be described in a subsequent paper.

¹www.vision-components.com

²MIPI CSI: Mobile Industry Processor Interface - Camera Serial Interface

³edmundoptics.fr/p/4mm-fl-f25-blue-series-m12-mu-videotrade-imaging-lens/31870/

⁴www.nxp.com

⁵www.ichaus.de

⁶digilent.com

⁷www.pjrc.com

E. Software

The Jetson TX2 runs a Ubuntu 20.04 aarch64 operating system with JetPack 5.1 SDK, the kernel is patched with MIPI CSI drivers from the camera manufacturer and loads a custom device tree. The cameras frames are captured using a custom C++ Python interface that access the low-level V4L2 API⁸. A acquisition and visualization GUI is built upon the *PyQTGraph* library⁹, data storage and processing is based on a custom library that wraps *h5py*¹⁰ and *OpenCV*¹¹, respectively. Parts of this software suite are released under an open source license alongside this article.

F. Lasers and Eye Safety Considerations

Working with lasers, especially in a data collection environment, requires care and caution. In particular, the use of diode lasers in the 850nm range are a safety concern as these wavelengths can reach the cornea and there is no blinking reflex as the light is mostly invisible. We use a pair of Digigram Technology PPR-CEE850-H68V53-30k laser dots projectors¹² that projects 30k points with a FoV of 67.7×53.4 degrees. These diode lasers have a rated output power of 200mW and are operated at 200mA yielding effective optical power of 200mW per projector, 100mW after the grating. These dots projectors use a frontal grating positioned approximately 10mm from the diode and generate a bundle of 30k laser points, the power per ray is of the order of $3\mu W$ and therefore too small to cause any eye damage by itself. The center zero-order mode however is more powerful, the datasheet claims that is below 0.2% of the total power, i.e. 0.4mW. We measured a slightly higher value of 0.5mW for the center mode, including neighboring points, using a Thorlabs PM160 Wireless Power Meter. This implies a Class 2 standard which is not be a problem for eye safety, especially since the lasers are activated for a 3ms time period, five times per capture. Moreover, we implemented additional safety measures in order to protect the subjects present for data collection, by closely monitoring laser power draw, by orienting the lasers so they are not directed in the subject and operator eyes, by taking regular measurement of the optical output and by training the operator to the specifics of the system.

IV. CALIBRATION, CAPTURE, PRE-PROCESSING AND STEREO RECONSTRUCTION

In order to test which technologies perform the best, the *sweet* sensor package has multiple cameras and illumination sources. In order to provide useful data for the algorithms, sensors, illumination and pre-processing pipelines should be precisely calibrated, a procedure described in this section.

A. Illumination and Light Field Calibration

The LEDs banks can be adjusted linearly along the z -axis and turned around the y -axis. Moreover, since the LEDs are individually addressable so the light intensity can be adjusted along the y -axis as well. In order to find the best vertical position, angle and individual LED intensity values we use a custom a ray-tracing software to predict the light intensity and perform a manual optimization *in situ* with a white paper target.

B. Camera Gain Calibration and Frame Alignment

When relative LEDs intensities and bank positions are set, the absolute intensity of the illumination, integration time and camera sensor gain should be setup to achieve the best possible performances. At 950nm both the LEDs and sensors have quite low performance which should be taken into account. The capture frame rate is fixed at 50Hz which leaves 20ms per frame to which should be subtracted the time for switching on and off the LEDs banks (2–3ms) as well as the sensor time to recover the image frame. In practice the maximum integration time is around 5ms with these parameters. In order to fix the sensor gain and the shutter time we perform a survey of noise vs gain and the optimal parameters we find is low gain (5dB) and medium integration time (2ms).

The specific camera sensors we have for this platform have a defect that a non deterministic number synchronization pulses (between 1 and 3 at 50Hz) are missed at the beginning of the capture. We develop a method consisting of two 10 frames binary patterns we call *claps* that are recorded at the beginning and at the end of the capture sequence, starting with 10 blank frames. A pre-processing routine then applies a simple pattern matching algorithm to recover the claps position, check that no frame were missed between those and trim away this data.

C. Camera Calibration and Sensors Characterization

It is essential for SV 3D reconstruction to have a very accurate characterization of the relative position of the stereo camera pair (extrinsic parameters), as well as a per camera projection matrix and lens distortion coefficients (intrinsic parameters). We perform two dozen of captures covering the whole FoV with a CharuCo target and extract the parameters with OpenCV. Intrinsic camera parameters are approximated with a 5 parameter lens distortion model and a camera matrix, while extrinsic parameters are given by a 3D rotation matrix and translation vector relative to the left camera.

D. Stereo Reconstruction and Camera Views Alignment

Reconstruction of the 3D depth map is done from a pair of rectified, un-distorted and aligned, left-right image pair. In particular, the calibration algorithm takes care that the rectification parameters, intrinsic and extrinsic, are tuned such that a point in 3D space appear at the same height in the image plane of the two cameras. If a point in 3D space appear at pixel positions x on the left image and x' on the right image, the difference is called the disparity

$$d = x - x' = \frac{Bf}{z}, \quad (5)$$

⁸V4L2

⁹PyQTGraph

¹⁰h5py

¹¹OpenCV

¹²Digigram

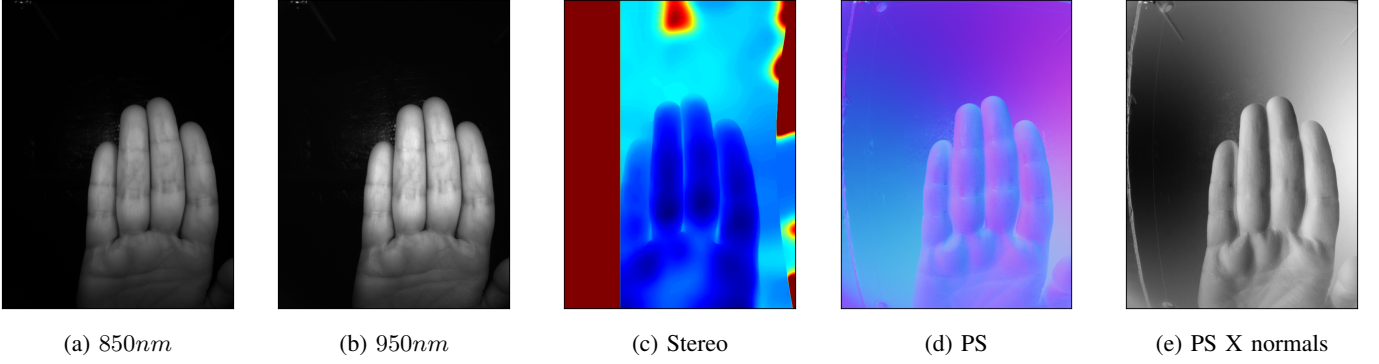


Fig. 4: Various channels for fingers.

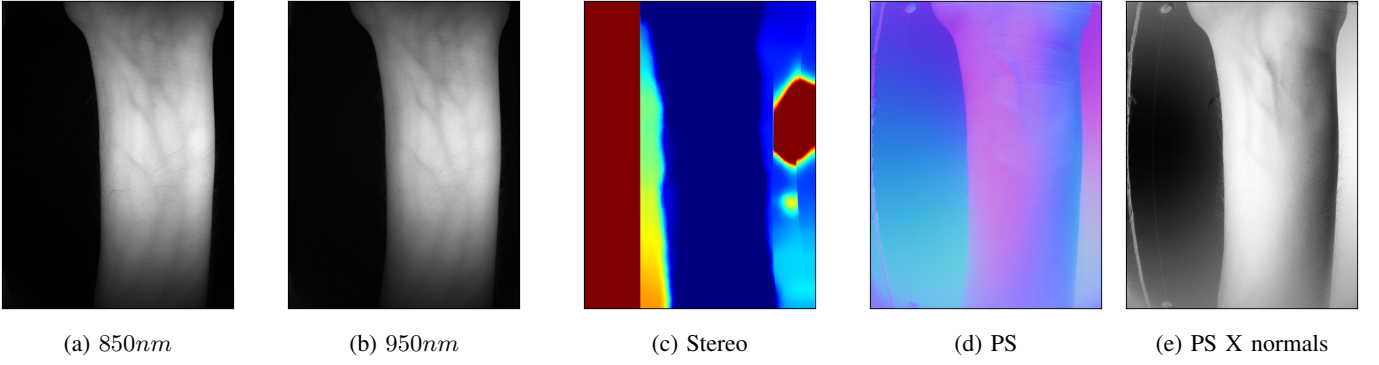


Fig. 5: Various channels for wrist

where B is the baseline distance between the two cameras, f is the focal length and z is the distance of the 3D point to the image plane. In order to find the disparity map, and depth map, a semi-global matching (SGM) algorithm using a mutual information (MI)-based pixel-wise matching algorithm [42] implemented in OpenCV (StereoSGBM). With this depth information we can align the RGB image pixel-wise with the reference left rectified view using a simple projection algorithm.

E. Photometric Stereo

We use a series of four images, taken with illumination from each corner of the LEDs banks respectively, as alternative way to extract a depth map known as Photometric Stereo (PS). It is possible to estimate the surface normals of the illuminated object using this technique proposed in [43]. The approach solves the least-square solution for the equation $I = L \cdot N$, with I the intensities observed in the images for each pixels, L the normalized vectors for each light sources and N the normal surfaces. Several assumptions are assumed to simplify the problem:

- The light vectors are assumed constant overall the image, such as emitted from infinitely distant isotropic sources.
- The hand skin is considered with a Lambertian reflectance model, without specular reflection.
- The hand surface is assumed smooth.

In addition to this algorithm, we perform a flat-field calibration to compensate the inverse square law of light propagation,

by using a flat reference with a constant albedo. This method makes the assumption that the hand is almost planar, its surface not deviating much from that of the reference plane.

V. VEIN RECOGNITION EXPERIMENTS



Fig. 6: Flowchart for constructing a FV-template from a FV-sample.

A biometrics based identity-verification system functions in two phases – *enrollment* and *probe*. Both phases operate on *biometric templates* – a template being a compact representation of a biometric sample. To enroll a new subject in the biometrics verification system, the subject provides a biometric sample. A template, constructed from this sample, is stored in the biometrics system, associated with the subject's identity. During the probe phase, the subject claims a certain identity, and provides a new biometric sample. The system then compares probe-template, derived from the probe-sample, with the template enrolled for the claimed identity. If the two templates are sufficiently similar (*i.e.*, the match-score is above a predetermined threshold), we consider that the claimed identity has been verified by the system. In this section we describe the template creation process, and then discuss the results of FV-recognition experiments with various protocols.

A. Finger-vein Template Creation

Figure 6 shows the flowchart of the FV-template creation process. Each input FV-sample is an image corresponds to a

presentation showing all fingers of the presented hand. First, the four fingers – index-, middle-, ring-, and little-finger – are segmented out from the input image. One template is constructed for each finger separately.

In the finger-segmentation step we process the input image to extract sub-images of individual fingers. To segment out each finger from an input image, first we generate a *foreground mask* using adaptive thresholding (Otsu’s method [44]) to detect the hand-region (foreground object) in the image. Morphological opening is used to delete small regions from the resulting binary image. We then scan the binary image along the horizontal axis for the first foreground pixel (assumed to belong to the hand in the image). The detected pixel corresponds to the tip of one finger (the tallest finger). This finger is then scanned along the direction perpendicular to the vertical axis of the finger. The left and right boundaries of the finger are obtained by scanning for finger-edges on both sides. This scanning process is repeated for each row in the image, as long as the left and right finger-boundaries extracted correspond to a reasonable finger-width. The scanning process terminates when the estimated finger-width becomes too large for a certain row in the image. At this point we assume that we have identified all pixels representing a single finger. Then we remove this finger from the image (set all finger-pixels to background) and repeat the scanning process again, this time to find another finger. This procedure is repeated for up to four times, to detect four fingers in the image.

By the nature of the finger-segmentation process, fingers are detected in order of their height in the input image (the finger closest to the top-edge of the image is detected first, followed by the second-tallest, and so on). In other words, the fingers are not necessarily extracted in the order index-to-little or the reverse. In further processing, we use the relative coordinates of the center-of-gravity of each finger-mask to reorder the fingers in a natural order from index to little. However, this finger-reordering procedure can be reliably applied only when all four fingers have been detected. (If, for example, only three fingers have been detected, then we cannot tell whether these are index, middle and ring fingers, or middle, ring, and little fingers.) For this reason, images where all four fingers are not detected, are excluded from further processing.

Next, a normalization step proposed by Huang *et al.* [35] is applied to each individual finger-image. This step simply rotates the finger-image to align the longitudinal axis of the finger to the vertical axis as best as possible.

The normalized finger-image is passed to the FV-enhancement module. Here we use a pre-trained autoencoder [40] to enhance the vascular structures in the input image. Preliminary experiments showed that FV-enhancement improves the FV recognition accuracy significantly. Hence, we have included the FV-enhancement module in our processing pipeline. A sample result of the vein enhancement process is shown in Figure 7.

FV patterns are compared based on a set of image-features extracted from the two vein-images being compared. In this work we have used the Maximum-Curvature (MC) features [34]. Here, the finger-vein image is scanned line by line in the direction transverse to the length of the finger. In each scan, the

pixels of high local curvature (local second derivative of pixel-values) along the line are marked as suitable feature-points. A sample result of the vein MC-feature-extraction process is shown in Figure 7(d). The MC feature-map extracted from an input FV-sample image is considered as the biometric template for the sample.

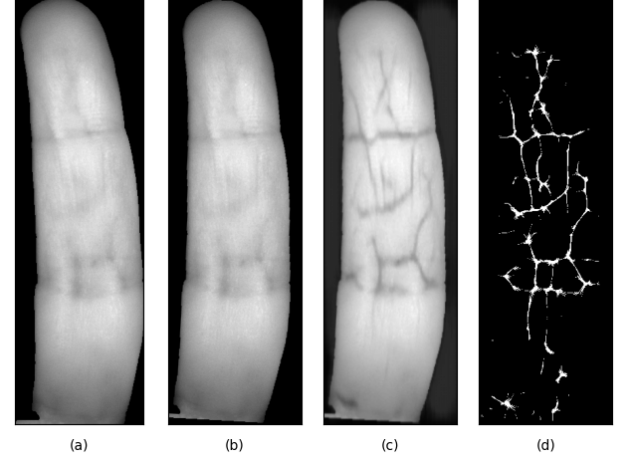


Fig. 7: Example result of the vein-enhancement. (a) Extracted finger-image; (b) normalized finger-image; (c) Vein-enhanced finger-image; (d) MC-feature-map extracted from (c). Note the slight rotation towards the vertical axis in (b) w.r.t. (a). The normalized finger-image, (b), forms the input to the vein-enhancement autoencoder.

B. Finger-vein Matching

We have used the method proposed by Miura *et al.* [34] to compare two MC-feature based templates. This method uses cross-correlation (computed in the frequency domain) to find the position of best match of the two input feature-maps. The cross-correlation coefficient at the best-match position is taken as the match-score between the two templates. In Section V-D we present experimental FVR results using mainly two ISO metrics: (1) False Match Rate (FMR) and (2) False Non-Match Rate (FNMR).

C. Dataset Construction

Using the *sweet* platform we have collected a dataset for FV recognition experiments. This dataset, named CandyFV, and the results of our FV recognition experiments are discussed in this section.

TABLE I: Age and gender distribution of 120 subjects represented in the CandyFV dataset. The first column indicates the age-groups in years.

Age-Group	Male	Female
18 – 30	22	19
31 – 50	20	18
51 and above	20	21
Total	62	58

FV samples from 120 subjects comprise the CandyFV dataset. For this dataset we attempted to have an even distribution of male and female subjects over three age ranges. The demographic distribution of the subjects who provided vein-biometrics samples for the CandyFV dataset is shown in Table I.

The dataset includes five samples for each hand of each subject. The subject presents the hand with four fingers close together (the *fingers-closed* modality), over the three cameras, at a distance of roughly 10cm – 12cm from the cameras. Thumbs may be entirely or partially visible in the samples; they are not used in our experiments.

Each sample includes 20 usable image-frames per camera, captured under a variety of illuminations. In particular, each sample yields three images captured under NIR-850nm for each of the two (left, right) NIR cameras, and similarly, three images captured under NIR-950 illumination.

D. Hand Recognition Experiments

We first discuss the results of several experiments for hand-identity verification based on individual fingers. Following that we present results of hand verification based on multiple fingers, using score-fusion in various ways.

1) *Single Finger Recognition*: FV templates have been compared under eight different protocols, described in Table II. Each protocol name is composed of three items: <Modality>_<Camera>_<NIR>. The Modality may be ‘LH’ (Left hand) or ‘RH’ (Right hand). The Camera component ‘left’ or ‘right’ indicates the NIR camera from which the template has been derived, and the NIR component may be ‘850’ or ‘950’, indicating the illumination used to capture the image-sample. Thus, with two options for each of three variables, we have eight different experimental protocols.

TABLE II: List of protocols under which finger-comparison experiments have been performed. For each protocol, the number of enrollment images and probe images in the development (Dev) set, as well as in the evaluation (Eval) set are also listed.

Id.	Protocol Name	Dev Set		Eval Set	
		Num. Images	Num. Images	Enrol.	Probe
P1	LH_left_850	159	8064	159	7836
P2	LH_left_950	141	4908	138	4665
P3	LH_right_850	159	7968	156	7791
P4	LH_right_950	147	6372	144	6300
P5	RH_left_850	156	7200	156	6998
P6	RH_left_950	153	6138	136	4644
P7	RH_right_850	156	7116	156	7032
P8	RH_right_950	144	4842	123	3969

For these experiments, first we partition the dataset into two subsets, named the *development* (‘Dev’) set and the *evaluation* (‘Eval’) set. The Dev set is used for tuning hyper-parameters of the finger-recognition system for the desired performance. The tuned recognition system is then applied to the data corresponding to the Eval set, to quantify the performance of the system. The Dev and Eval sets have been constructed arbitrarily, based on the numerical subject-id assigned to each subject. Data for the first 60 subjects has been assigned to the Dev set and data for the remaining subjects has been assigned to the Eval set.

From each image captured by the *sweet* platform, we extract three individual finger-vein images, corresponding to the index-, middle- and ring-finger recorded in the image. Within each set (Dev or Eval), we have five samples for each user, for each modality. Typically, in each sample, for each

camera (left, right), we have three NIR-850nm images and three NIR-950 images. That is, in total, for each camera we have 15 NIR-850 images per subject, and similarly 15 NIR-950 images. Thus, for each of 60 subjects in each partition, we have 45 finger-vein images for each camera and each NIR-illumination.

The next step is to construct enrolment-sets and probe-sets. Here, we have arbitrarily selected one sample for each modality of each subject for the enrolment sample. The remaining samples have been designated as probe-samples. For the finger-vein recognition experiments, each enrolled sample is considered a unique identity.

Each probe-sample has been used for four comparisons – one genuine comparison (with the correctly matched identity), and three *zero-effort-impostor* (ZEI) comparisons (with non-matched identities). In each ZEI comparison, the claimed-identity for a given probe template is selected randomly. For each protocol, the number of enrolled samples and probe-samples in each set (Dev or Eval) are shown in Table II. We note two points from the Table:

- 1) the number of enrollment and probe samples for the protocols with NIR-950 illumination are consistently smaller than those for the NIR-850 protocols;
- 2) the numbers of images used for enrolment are not exactly 180 (three fingers for 60 subjects each).

Both observations can be explained by the finger-segmentation results. Images where the finger-segmentation step failed to detect exactly four fingers have been excluded from these experiments. We noted that there were significantly more finger-segmentation errors for images captured with the NIR-950 illumination, than those captured under the NIR-850 illumination.

We estimate the finger-vein recognition rates for a specific FMR of 0.1%.¹³ In this analysis, the score-threshold is selected such that the FMR over the Dev set does not exceed the desired FMR. This score-threshold is then applied the Dev set and the Eval set, to determine the actual FMR and FNMR rates over each dataset.

In Table III¹⁴ we summarize the FMR and FNMR achieved for various evaluation protocols, for single finger recognition, for the FMR ceiling of 0.1%.

Table III shows that the FVR performance is significantly better for the right-hand fingers than for the left-hand fingers. We do not have any logical explanation for this phenomenon. This has probably happened for one of two reasons:

- 1) increased familiarity with the data-capture procedure – subjects were consistently asked to present the left-hand first, therefore, presentations with the right-hand may have been ‘better’, or
- 2) simply due to right-handedness of most subjects, which may lead to smaller variability in right-hand data, compared to left-hand data.

¹³The actual FMR achieved over the Dev set may be slightly lower than the desired FMR of 0.1%. This happens because, if the classification-score threshold were selected so as to allow even one additional false-match, then the FMR over the Dev set would exceed 0.1%.

¹⁴In all the result-tables here, the FMR, FNMR and HTER values are expressed as percentages.

TABLE III: Finger-vein recognition performance at False-Match rate (FMR) of 0.1%. The score-threshold has been computed to achieve the desired FMR (0.1%) on the Dev set. This score-threshold is then applied to the FVR scores from the Eval set. The lowest HTER value is highlighted in bold characters, and corresponds to the RH_right_850 protocol. In general the performance for all the right-hand protocols is significantly lower than for the left-hand protocols.

Protocol	Dev Set			Eval Set		
	FMR	FNMR	HTER	FMR	FNMR	HTER
P1	0.1	3.82	1.96	0.17	7.3	3.74
P2	0.08	8.7	4.39	0.09	10.05	5.07
P3	0.08	5.77	2.93	0.0	6.46	3.23
P4	0.09	7.74	3.91	0.02	9.45	4.74
P5	0.09	0.66	0.38	0.79	0.61	0.7
P6	0.09	0.57	0.33	0.66	0.60	0.63
P7	0.09	0.33	0.21	0.68	0.45	0.57
P8	0.09	1.39	0.74	0.04	2.27	1.15

We also note that the recognition-rates achieved for protocols involving 850 nm NIR illumination are usually somewhat better than the corresponding (*i.e.*, same hand, same camera) protocols involving 950 nm illumination. This result is counterintuitive. In theory, we expect 950 nm illumination to provide better results than 850 nm, because 950 nm NIR penetrates the soft-tissue of the fingers to a deeper extent than 850 nm NIR. Also, 850 nm NIR tends to produce more speckle noise on the skin-surface. On the other hand, much more power is needed for the 950 nm illumination. Our conjecture is that the *sweet* platform might not have sufficient power for the 950 nm illumination to provide the expected results.

2) *Hand-Recognition Based on Finger-Score Fusion*: In the experiments discussed so far, each finger has been considered a unique identity, that is, the identity of a subject is verified based on only a single finger at a time. Next, we consider each hand of a subject as a unique identity, and attempt to validate the identity of each hand based on combined recognition of three fingers of the hand – the index-finger, the middle-finger, and the ring-finger. The raw scores used for single-finger recognition can be combined to recognize a hand based on the vascular patterns of the three fingers combined. For each hand, the scores the three fingers obtained in each of the eight protocols (Table II) are combined. Thus, each hand-probe is represented by a 3-dimensional (3-D) feature-vector.¹⁵

The general approach to score-fusion adopted in this study is as follows: feature-vectors are constructed for each hand-identity using the individual finger-comparison scores. While constructing these feature-vectors, finger-scores are selected either only from genuine-probes, or only from ZEI-probes. In this way we obtain, for each hand-identity, a set of genuine-probe (‘match’) feature-vectors, and another set of ZEI (‘non-match’) feature-vectors. A two-class classifier is

¹⁵Besides finger-fusion, we also experimented with camera-fusion, wavelength-fusion, as well as fusion of both cameras and both NIR illuminations all together, for three fingers of each hand. However, these score-fusion strategies did not bring any further improvement to hand-recognition performance, over simple finger-fusion. There may be two reasons for the lack of performance improvement: (1) the information captured by the two cameras, or under the two kinds of NIR illumination may not be sufficiently complementary; or (2) we probably do not have sufficient data to train the respective two-class classifiers for the camera-fusion and wavelength-fusion studies. Therefore, due to lack of space, we have not discussed these score-fusion experiments here.

then constructed using the feature-vectors in the Dev set. This classifier is used to label the feature-vectors of the Eval set, to quantify the hand-recognition performance of the system. In this study, we have used Support Vector Machines (SVM) with RBF (radial basis function) kernels, for the score-fusion experiments.

In each protocol in Table II, we fuse the FVR-scores of the three fingers of the hand corresponding to the protocol. Thus, all probe feature-vectors used in a given experiment represent information from the same hand, captured by the same NIR camera, under the same NIR illumination. The results of FVR-score fusion within each FVR protocol are shown in Table IV. These numbers quantify the performance of the score-fusion system when the FMR over the Dev set is limited to 0.1%. That is, the classification-score threshold¹⁶ is selected in such a way that the FMR over the Dev set does not exceed 0.1%. This classification-score-threshold is then applied to the classification-scores generated for the Eval set, to estimate the FMR and FNMR over the Eval set.

TABLE IV: Results of score-fusion of three fingers of a hand within the same protocol. The best performance, printed in bold, corresponds to the protocol ‘RH_right_850’.

Prot-ocol	Dev Set			Eval Set		
	FMR	FNMR	HTER	FMR	FNMR	HTER
P1	0.1	2.68	1.39	0.20	4.29	2.25
P2	0.08	4.2	2.14	0.54	3.57	2.06
P3	0.05	2.71	1.38	0.05	3.93	1.99
P4	0.06	3.04	1.55	0.6	2.67	1.66
P5	0.06	0.0	0.03	0.46	0.0	0.23
P6	0.07	0.0	0.03	0.45	0.0	0.23
P7	0.06	0.0	0.03	0.11	0.0	0.06
P8	0.08	0.46	0.27	0.0	1.51	0.76

First, we note that FVR-score fusion improves the hand-recognition performance compared to single finger FVR. For the left hand, the single FVR error-rates (HTER in Table III), range from 3.5% to 5% for each of the individual fingers. Finger-fusion reduces the left-hand recognition error-rates to about 2% or lower in all four left-hand protocols. For the right-hand, single-finger FVR performance is already very high (FVR in protocols P5 – P8 in Table III). Multi-finger FVR performance for the right hand still reduces the classification error. The best performance, a HTER of 0.06% for the ‘RH_right_850’, is a 10-fold improvement over single-finger FVR in the same protocol.

VI. CONCLUDING REMARKS

In this paper we have described the design of a contactless vascular biometrics platform named *sweet*, that has been developed for the purpose of testing of various technologies and methods for contactless vascular biometrics. With this platform we can record hand vascular images in NIR wavelengths (850 and 950 nm) and skin surface in in color RGB. With a pair of NIR cameras and by varying illumination incidence angle we

¹⁶Note that, for the fusion experiments, the score-thresholds are not the raw finger-scores, but the scores generated by the SVM classifier for each probe. To avoid confusion, in these fusion experiments we refer to the threshold applied to the output of the 2-class classifier as the ‘classification-score-threshold’.

can also extract precise and detailed depth and surface-normal maps using SV and PS, respectively.

In this work we have focussed on finger-vein (FV) biometrics using this platform. Unlike existing FV sensors that capture vascular data from only one finger at a time, the *sweet* platform is designed to image four fingers of a hand simultaneously. This enables us to implement multi-finger vein recognition, which is not possible using previous FV devices.

We have collected a large dataset of vascular biometrics samples from 120 subjects. The FV data collected from these subjects has been curated into a dataset named CandyFV. In this paper we report FV recognition results based on this dataset.

We start with FV recognition experiments where each finger of a subject is treated as a unique identity. Only images of the index-, middle-, and ring-finger of each hand have been included in these experiments. For each finger we have eight test protocols – all possible combinations of two hands, two cameras, and illumination using two NIR-wavelengths. A probe-sample is compared to an enrolled reference using the Miura-Match method based on maximum-curvature (MC) vein features [34]. In all experiments the finger-veins have first been enhanced using an autoencoder based method [40].

We found that the data for the right hand provides better FV recognition results than the left hand. In particular, the best single finger recognition result (HTER of 0.6%) has been achieved for the right hand using data captured by the right NIR camera under 850 nm illumination. (See Table III.) We do not see any systematic reason why the FVR results for the right hand should be better than those for the left hand. Perhaps, because most subjects are right handed, the data recorded for the right hands of subjects may have smaller variability.

Next we have explored score-fusion, to combine information from multiple fingers, to identify a hand. In these score-fusion experiments, each hand is considered as a unique identity, represented by three fingers. The FVR scores for the three fingers the hand are used to construct a feature-vector representing the hand. A two-class support vector machine (SVM) classifier is then trained to verify the identity of the presented hand.

Fusing the scores of the three fingers within each protocol (same camera, same wavelength), we can achieve a hand-recognition error rate of 0.06% (a 10-fold improvement over the error-rate of recognition based on only one finger).

Our platform has been designed in a modular fashion and allows for a large range of improvements and extensions. In the future we will extend this platform in several ways to improve its acquisition performances, for instance by adding side facing cameras, adding sensors with better performance in the NIR range and by experimenting with illumination, for example using polarized light. We also want to test other technologies, such as Single Pixel Laser Detectors (SPLD) to add capabilities in the SWIR range. We will also improve the pre-processing pipeline with channel fusion such as SV with PS fusion. Moreover, the fast acquisition frame-rate facilitates even more complex algorithms based on image sequence analysis, which we will explore in the future.

The CandyFV dataset offers a large scope for further research.

Fusion: Up to now we have only explored score-based fusion. This strategy worked well for combining multiple fingers, but did not lead to further performance-improvement when applied to camera fusion or NIR-wavelength fusion. Next we aim to study data-fusion and feature-fusion methods for combining information from the two NIR cameras, as well as from the two NIR illumination wavelengths.

End-to-end processing: Our initial experiments with CNN based end-to-end FV recognition have not shown results comparable to those presented in this report. This is why end-to-end FV recognition has not been discussed here. In future work we plan to explore this direction more rigorously.

ACKNOWLEDGEMENT

This work has been supported by the Innosuisse project CANDY, in collaboration with GlobalID. The authors also gratefully acknowledge the contributions of Ms. Karine Vaucher, Mr. Victor Bros, Mr. J  r  my Maceiras, Mr. Vincent Pollet, and Mr. Bastien Crettol – all members of Idiap staff. They contributed various software packages used in this work, helped with data-collection and other experiments.

REFERENCES

- [1] L. Wang and G. Leedham, "Near- and far-infrared imaging for vein pattern biometrics," in *2006 IEEE International Conference on Video and Signal Based Surveillance*. IEEE, 2006, pp. 52–52.
- [2] J. Hashimoto, "Finger vein authentication technology and its future," in *2006 Symposium on VLSI Circuits, 2006. Digest of Technical Papers*. IEEE, 2006, pp. 5–8.
- [3] K. Shaheed *et al.*, "A systematic review of finger vein recognition techniques," *Information*, vol. 9, no. 9, p. 213, 2018.
- [4] M. Vanoni *et al.*, "Cross-database evaluation using an open finger vein sensor," in *2014 IEEE workshop on biometric measurements and systems for security and medical applications (BIOMS) proceedings*. IEEE, 2014, pp. 30–35.
- [5] A. H. Mohsin *et al.*, "Finger vein biometrics: taxonomy analysis, open challenges, future directions, and recommended solution for decentralised network architectures," *IEEE Access*, vol. 8, pp. 9821–9845, 2020.
- [6] R. Raghavendra *et al.*, "Design and development of low-cost sensor to capture ventral and dorsal finger vein for biometric authentication," *IEEE Sensors Journal*, vol. 19, no. 15, pp. 6102–6111, 2019.
- [7] J. A. Otter *et al.*, "Evidence that contaminated surfaces contribute to the transmission of hospital pathogens and an overview of strategies to address contaminated surfaces in hospital settings," *American Journal of Infection Control*, vol. 41, no. 5, pp. S6–S11, 2013.
- [8] R. Raghavendra *et al.*, "A low-cost multi-fingervein verification system," in *2018 IEEE International Conference on Imaging Systems and Techniques (IST)*. IEEE, 2018, pp. 1–6.
- [9] G. K. O. Michael *et al.*, "Design and implementation of a contactless palm print and palm vein sensor," in *2010 11th International Conference on Control Automation Robotics & Vision*. IEEE, 2010, pp. 1268–1273.
- [10] Z. Zhang, F. Zhong, and W. Kang, "Study on reflection-based imaging finger vein recognition," *IEEE Transactions on Information Forensics and Security*, vol. 17, pp. 2298–2310, 2021.
- [11] P. Tome and S. Marcel, "Palm vein database and experimental framework for reproducible research," in *2015 international conference of the biometrics special interest group (BIOSIG)*. IEEE, 2015, pp. 1–7.
- [12] P. Chen *et al.*, "Design of low-cost personal identification system that uses combined palm vein and palmprint biometric features," *IEEE Access*, vol. 7, pp. 15922–15931, 2019.
- [13] A. Sierro, P. Ferrez, and P. Roduit, "Contact-less palm/finger vein biometrics," in *2015 International Conference of the Biometrics Special Interest Group (BIOSIG)*. IEEE, 2015, pp. 1–12.
- [14] R. Raghavendra and C. Busch, "A low cost wrist vein sensor for biometric authentication," in *2016 IEEE International Conference on Imaging Systems and Techniques (IST)*. IEEE, 2016, pp. 201–205.

- [15] S. Bhattacharya, A. Ranjan, and M. Reza, "A portable biometrics system based on forehead subcutaneous vein pattern and periocular biometric pattern," *IEEE Sensors Journal*, vol. 22, no. 7, pp. 7022–7033, 2022.
- [16] W. Yuan and Y. Tang, "The driver authentication device based on the characteristics of palmprint and palm vein," in *2011 International Conference on Hand-Based Biometrics*. IEEE, 2011, pp. 1–5.
- [17] D. Zhang, Z. Guo, and Y. Gong, "Multispectral biometrics systems," in *Multispectral biometrics*. Springer, 2016, pp. 23–35.
- [18] L. Spinoulas *et al.*, "Multispectral biometrics system framework: Application to presentation attack detection," *IEEE Sensors Journal*, vol. 21, no. 13, pp. 15 022–15 041, 2021.
- [19] S. Crihalmeanu and A. Ross, "Multispectral scleral patterns for ocular biometric recognition," *Pattern Recognition Letters*, vol. 33, no. 14, pp. 1860–1869, 2012.
- [20] R. Rowe, K. Nixon, and S. Corcoran, "Multispectral fingerprint biometrics," in *Proceedings from the Sixth Annual IEEE SMC Information Assurance Workshop*, 2005, pp. 14–20.
- [21] Y. Hao *et al.*, "Multispectral palm image fusion for accurate contact-free palmprint recognition," in *2008 15th IEEE International Conference on Image Processing*. IEEE, 2008, pp. 281–284.
- [22] K. I. Chang *et al.*, "Multimodal 2d and 3d biometrics for face recognition," in *2003 IEEE International SOI Conference. Proceedings (Cat. No. 03CH37443)*. IEEE, 2003, pp. 187–194.
- [23] X. Liang *et al.*, "Innovative contactless palmprint recognition system based on dual-camera alignment," *IEEE Transactions on Systems, Man, and Cybernetics: Systems*, vol. 52, no. 10, pp. 6464–6476, 2022.
- [24] C. Kauba *et al.*, "Three-dimensional finger vein recognition: A novel mirror-based imaging device," *Journal of Imaging*, vol. 8, no. 5, 2022.
- [25] W. Kang *et al.*, "Study of a full-view 3d finger vein verification technique," *IEEE Transactions on Information Forensics and Security*, vol. 15, pp. 1175–1189, 2019.
- [26] K. H. Cheng and A. Kumar, "Contactless biometric identification using 3d finger knuckle patterns," *IEEE transactions on pattern analysis and machine intelligence*, vol. 42, no. 8, pp. 1868–1883, 2019.
- [27] L. Chen, X. Wang, H. Jiang, L. Tang, Z. Li, and Y. Du, "Design of palm vein platform and pattern enhancement model based on raspberry pi," in *2021 IEEE International Conference on Emergency Science and Information Technology (ICESIT)*. IEEE, 2021, pp. 495–498.
- [28] I. P. A. S. Gunawan *et al.*, "Vein visualization system using camera and projector based on distance sensor," in *2018 International Electronics Symposium on Engineering Technology and Applications (IES-ETA)*. IEEE, 2018, pp. 150–156.
- [29] Y. Yin *et al.*, "SDUMLA-HMT: A multimodal biometric database," in *Biometric Recognition*. Springer Berlin Heidelberg, 2011, pp. 260–268.
- [30] Y. Lu *et al.*, "An available database for the research of finger vein recognition," vol. 1, 12 2013, pp. 410–415.
- [31] B. T. Ton and R. N. J. Veldhuis, "A high quality finger vascular pattern dataset collected using a custom designed capturing device," in *Proc. 2013 Intl. Conf. on Biometrics (ICB)*, 2013, pp. 1–5.
- [32] X. Qiu, W. Kang, S. Tian, W. Jia, and Z. Huang, "Finger vein presentation attack detection using total variation decomposition," *IEEE Transactions on Information Forensics and Security*, vol. 13, no. 2, pp. 465–477, 2018.
- [33] M. Miura, A. Nagasaka, and T. Miyatake, "Feature Extraction of finger-vein patterns based on repeated line tracking and its Application to Personal Identification," in *Proceedings on IAPR conference on Machine Vision and Applications*, vol. 15, 2004, pp. 194 – 203.
- [34] —, "Extraction of Finger-Vein Pattern Using Maximum Curvature Points in Image Profiles," in *Proceedings on IAPR conference on Machine Vision Applications*, 2005, pp. 347–350.
- [35] B. Huang *et al.*, "Finger-vein authentication based on wide line detector and pattern normalization," in *2010 20th International Conference on Pattern Recognition*, 2010, pp. 1269–1272.
- [36] J. Yang, Y. Shi, and R. Wu, "Finger-vein recognition based on gabor features," in *Biometric Systems*, Z. Riaz, Ed. Rijeka: IntechOpen, 2011, ch. 2. [Online]. Available: <https://doi.org/10.5772/17182>
- [37] I. Kovač and P. Marák, "Finger vein recognition: utilization of adaptive gabor filters in the enhancement stage combined with sift/surf-based feature extraction," *Signal, Image and Video Processing*, vol. 17, pp. 635 – 641, 2023.
- [38] H. Bay *et al.*, "SURF: Speeded up robust features," *Computer Vision and Image Understanding (CVIU)*, vol. 110, no. 3, pp. 346–359, 2008.
- [39] R. Zhang *et al.*, "Deep learning for finger vein recognition: A brief survey of recent trend," 07 2022. [Online]. Available: <https://arxiv.org/pdf/2207.02148.pdf>
- [40] V. Bros, K. Kotwal, and S. Marcel, "Vein enhancement with deep auto-encoders to improve finger vein recognition," in *Biometrics Special Interest Group (BIOSIG 2021)*, 2021.
- [41] K. Kotwal and S. Marcel, "Residual feature pyramid network for enhancement of vascular patterns," in *Proceedings of the IEEE/CVF Conference on Computer Vision and Pattern Recognition (CVPR) Workshops*, June 2022, pp. 1588–1595.
- [42] H. Hirschmüller, "Stereo processing by semiglobal matching and mutual information," *IEEE Transactions on Pattern Analysis and Machine Intelligence*, vol. 30, no. 2, pp. 328–341, 2008.
- [43] R. J. Woodham, "Photometric method for determining surface orientation from multiple images," *Optical Engineering*, vol. 19, no. 1, pp. 139–144, 1980.
- [44] N. Otsu, "A threshold selection method from gray-level histograms," *IEEE Transactions on Systems, Man, and Cybernetics*, vol. 9, no. 1, pp. 62–66, 1979.